Supplementary information:

Phosphorus-doped amorphous TiO_2/C interface enables hierarchical SEI formation on micron-sized SiO anodes for ultra-stable lithium-ion batteries

Xiuyan Liu, Jinjun Zhou, Guanjia Zhu,* Jihao Li, Haijiao Zhang*

Institute of Nanochemistry and Nanobiology, School of Environmental and Chemical Engineering, Shanghai University, Shanghai 200444, P. R. China

*Corresponding author

E-mail: zhuguanjia@shu.edu.cn; hjzhang128@shu.edu.cn

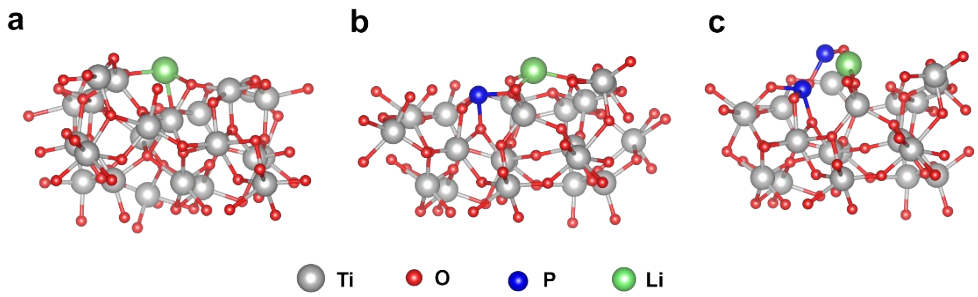

Fig. S1 Li^+ adsorption modes of (a) a-TiO_2, (b) a-TiO_2-P, (c) a-TiO_2-2P

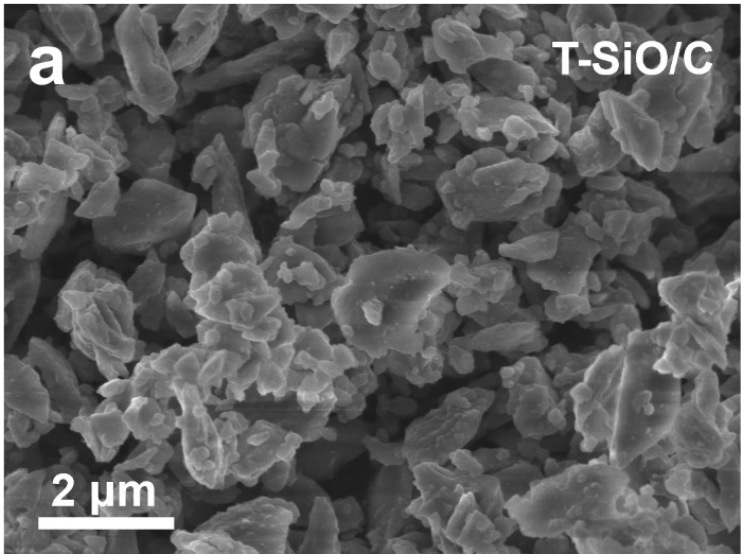

Fig. S2 SEM image of (a) T-SiO/C.

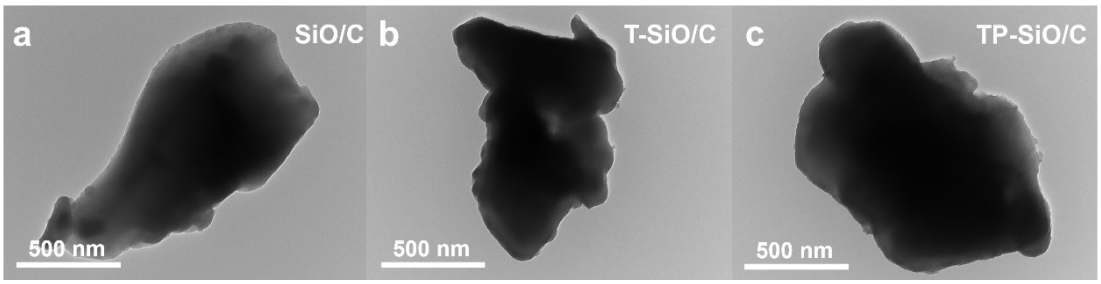

Fig. S3 TEM images of (a) SiO/C, (b) T-SiO/C, and (c) TP-SiO/C.

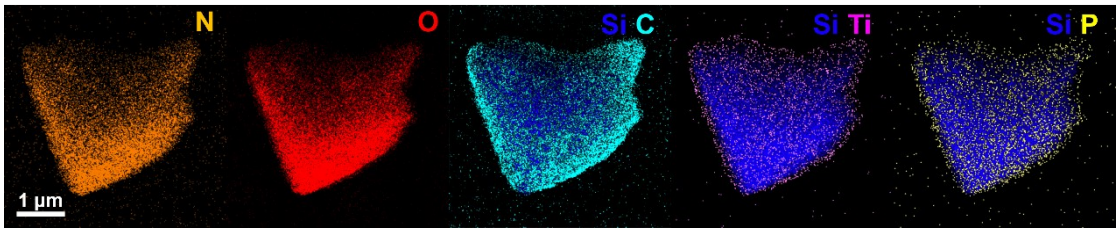

Fig. S4 EDS mapping images of TP- SiO/C

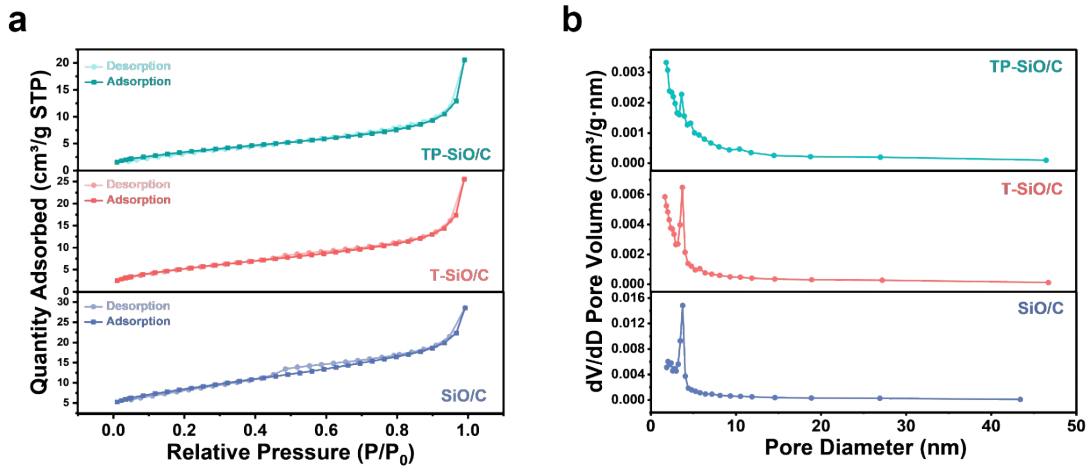

Fig. S5 (a) Nitrogen adsorption/desorption isotherms TP-SiO/C, T-SiO/C, and SiO/C. (b) Barrett-Joyner-Halenda (BJH) pore size distribution curves of TP-SiO/C, T-SiO/C, and SiO/C.

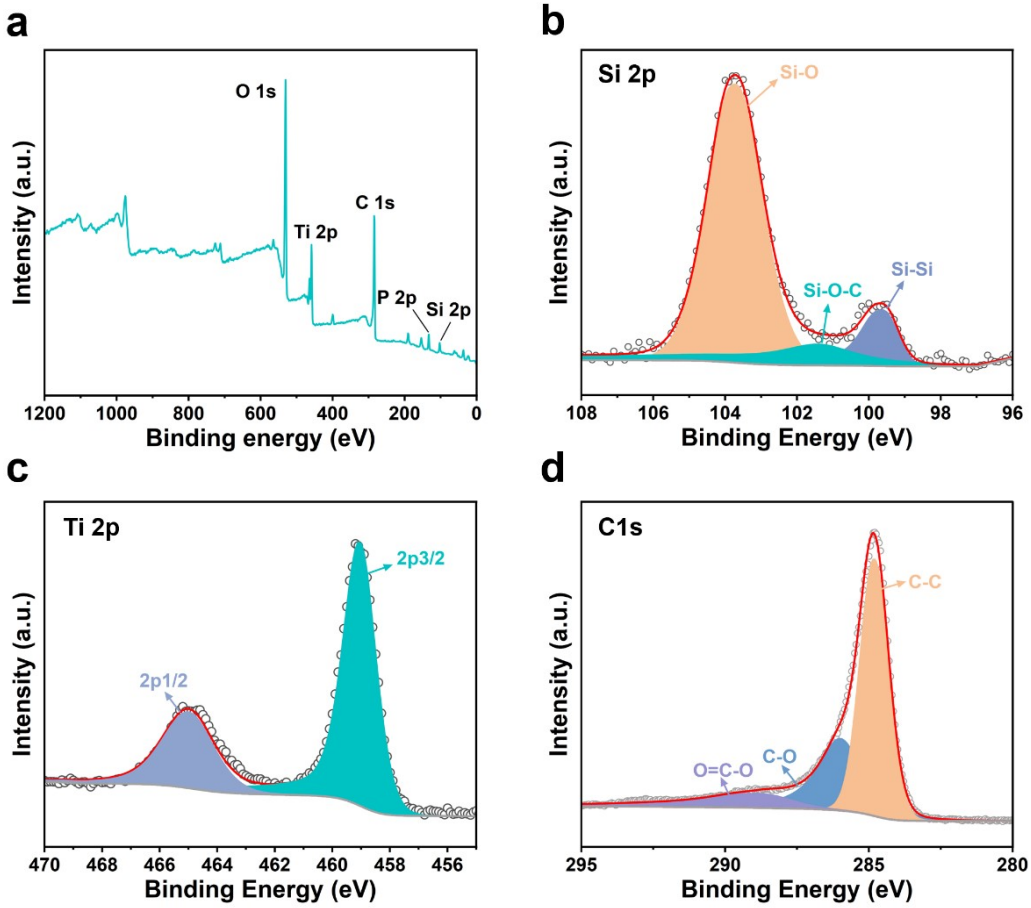

Fig. S6 (a) XPS survey spectrum of the TP-SiO/C. High-resolution XPS (b) Si 2p, (c) Ti 2p, and (d) C 1s spectra.

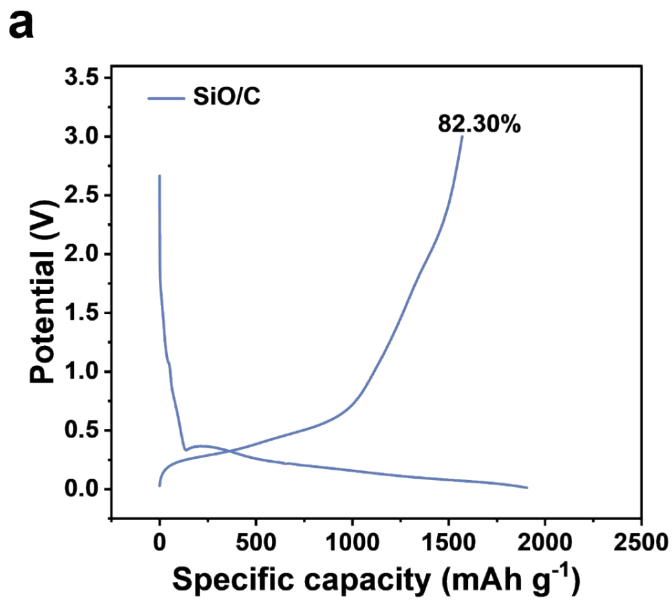

Fig. S7 The initial discharge/charge curves of SiO/C electrode

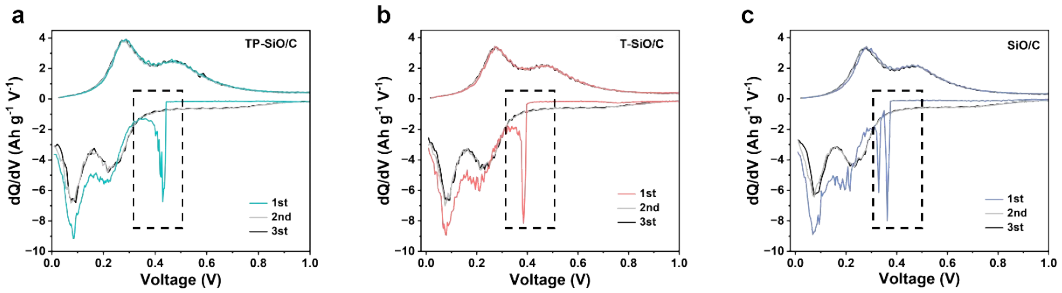

Fig. S8 dQ/dV curves of (a) TP-SiO/C, (b) T-SiO/C, and (c) SiO/C in the 1st–3rd cycles

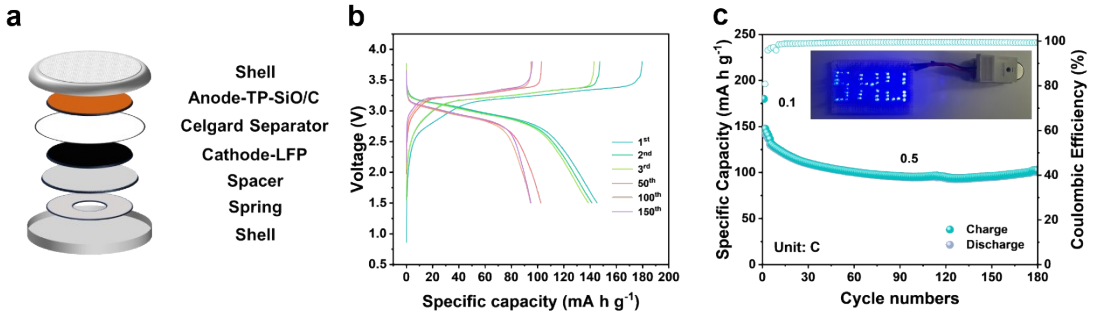

Fig. S9 (a) Schematic illustration of the TP-SiO/C//LFP full-cell. (b) Galvanostatic charge/discharge profiles and (c) cycling performance of TP-SiO/C//LFP full-cell (inset is the lighting of a digital photo of the LED device with the “LIB” pattern).

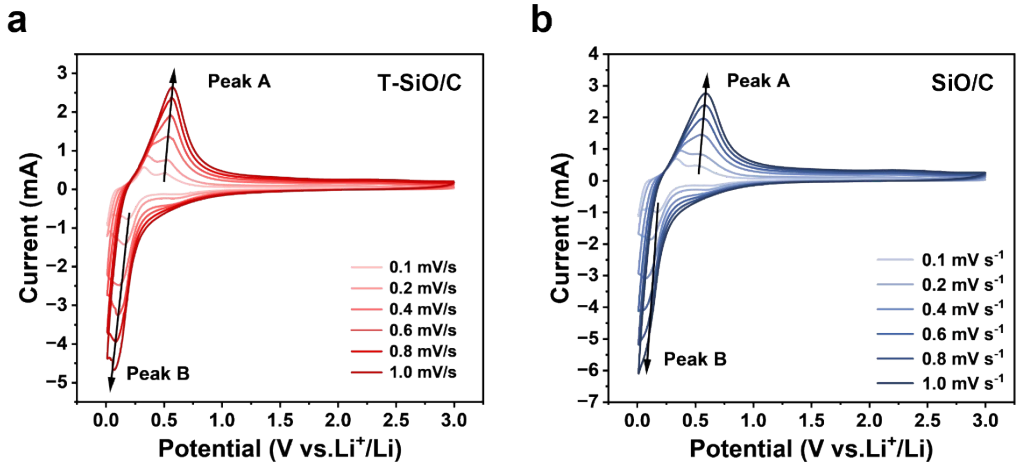

Fig. S10 CV curves of (a) T-SiO/C, (b) SiO/C at different scan rates of 0.1−1.0 mV s^{-1}

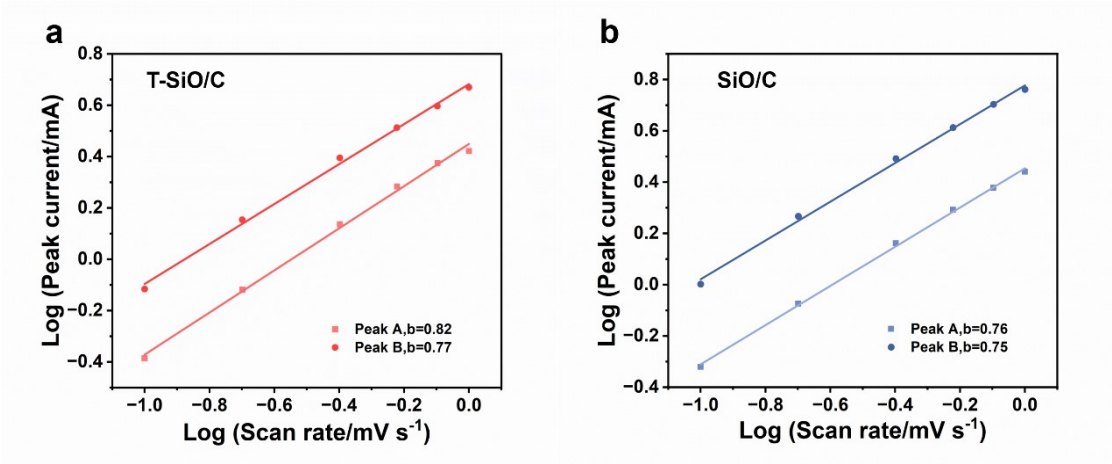

Fig. S11 Correlation between the logarithm of the peak current and the logarithm of the sweep frequency of (a) T-SiO/C, (b) SiO/C

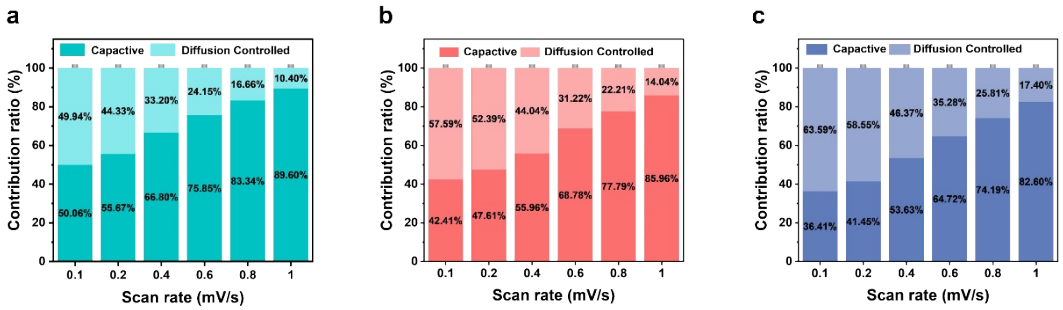

Fig. S12 Contribution ratio of the pseudo capacitance and diffusion contribution at different scan rates of the (a) TP-SiO/C, (b) T-SiO/C, and (c) SiO/C electrodes.

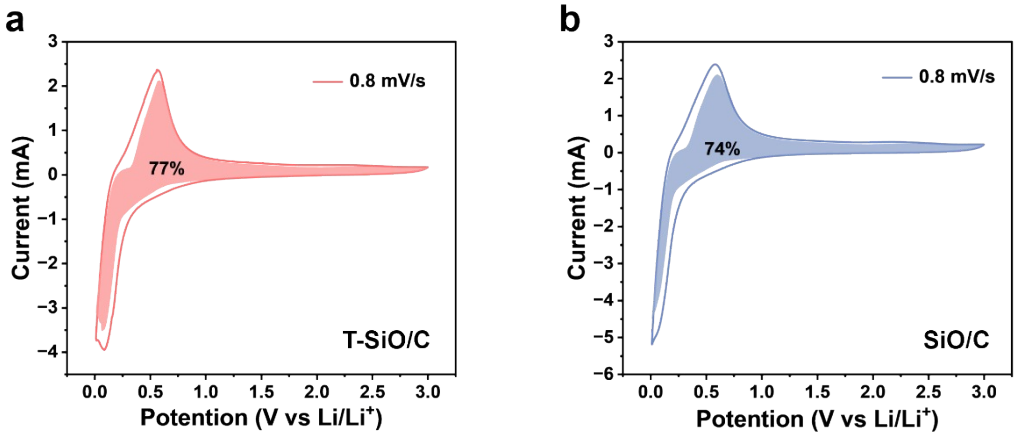

Fig. S13 Contribution of capacitive charge storage to the total capacity of (a) T-SiO/C and (b) SiO/C electrodes at a scan rate of 0.8 mV s^{-1}.

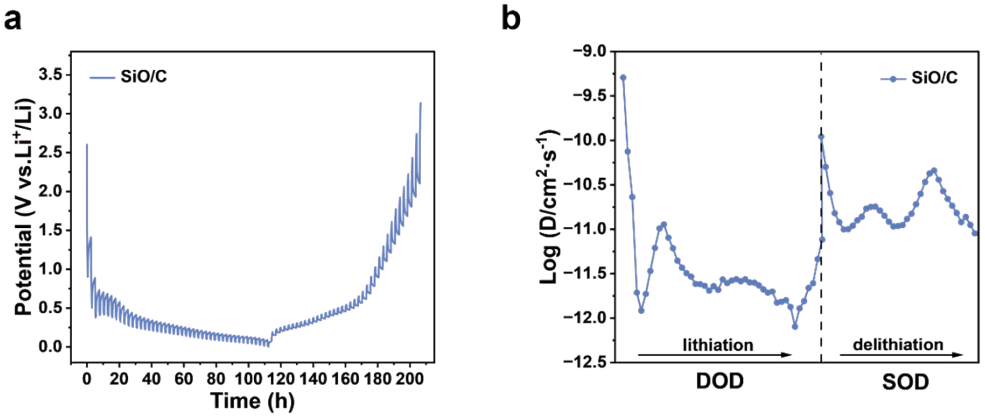

Fig. S14 (a) GITT curves of SiO/C. (b) Li^+ diffusion rate in different DOD/SOC of SiO/C.

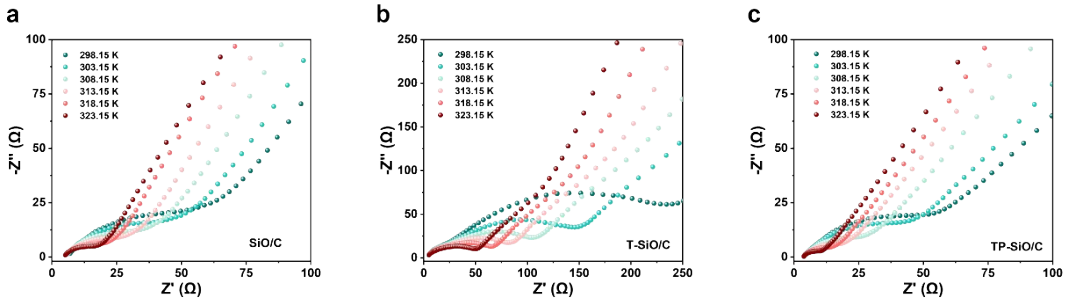

Fig. S15 The EIS spectra at different temperatures of (a) SiO/C, (b) T-SiO/C, (C) TP-SiO/C

To investigate the Li^+ transport kinetics at the interface, electrochemical impedance spectroscopy (EIS) of the cycled TP-SiO/C, T-SiO/C, and SiO/C electrodes was measured at temperatures ranging from 25°C to 50°C. Before testing, the coin cells were equilibrated at each temperature for 30 minutes to ensure thermal stability. The related activation energies (E_a) were obtained by fitting the EIS at different temperatures. Based on the law of Arrhenius:

$$\frac{T}{R} = Aexp^{(-\frac{E_a}{RT})}$$

Where T is the temperature, R is the fitted resistance, A is the pre-exponential factor,

E_a is the activation , R is 8.314 J (mol K)$^{-1}$.

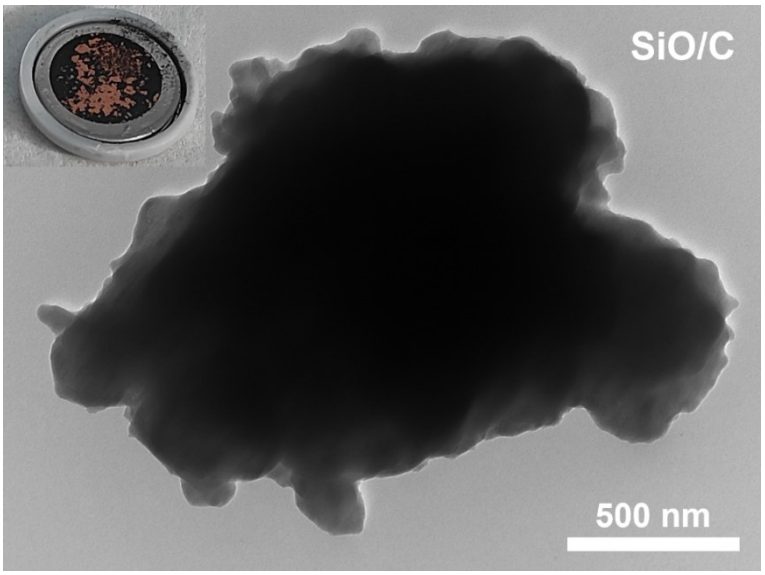

Fig. S16 Optical photograph and TEM image of SiO/C after cycles

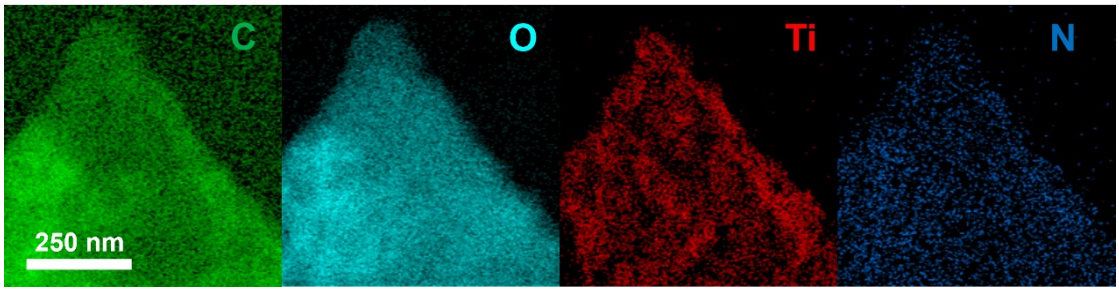

Fig. S17 EDS mapping images of TP-SiO/C after cycles.

Table S1. Comparison of the electrochemical performances of the TP-SiO/C electrode with other SiO-based anodes for lithium-ion batteries.

Materials	**Current Density (A g^{-1})**	**Cycles**	**Specific Capacity (mAh g^{-1})**	**Ref.**
TP-SiO/C	2	500	730.9	This work

p-SiO_x@0.3TiO_2@C	0.7	500	588.2	Ref.31
m-SiOx/C/MXene	1	400	918	Ref.32
SiO_x-TiON-200	0.5	250	854	Ref.33
SiOG@LiF3	1.5	500	706	Ref.34
SiO_x@Fe_3O_4@FLG	0.5	500	833.4	Ref.13
SiO_x@CoC	1	350	1044	Ref.35
SiO_x-Co@C	0.5	500	653.2	Ref.36
SiO@C@CoO	1	760	714.8	Ref.12
SSBCN	1	400	1151.3	Ref.9
(SiO_x/TiO_2)@CN	1	500	547	Ref.37
SiO_x@TiO_2@C	1	600	1197.8	Ref.11